Polaronic Conductivity in the Photoinduced Phase of $1T$-TaS_2

N. Dean,[1,*] J. C. Petersen,[1,2] D. Fausti,[1,2] R. I. Tobey,[1,3] S. Kaiser,[2] L. V. Gasparov,[4] H. Berger,[5] and A. Cavalleri[1,2,†]

[1]*Department of Physics, University of Oxford, Clarendon Laboratory, Parks Road, Oxford, OX1 3PU, United Kingdom*

[2]*Max Planck Department for Structural Dynamics, University of Hamburg, Centre for Free Electron Laser Science, Notkestraße 85, 22607 Hamburg, Germany*

[3]*Condensed Matter Physics and Material Sciences Department, Brookhaven National Laboratory, Upton, New York 11973, USA*

[4]*Department of Chemistry and Physics, University of North Florida, 4567 St. Johns Bluff Road, South Jacksonville, Florida 32224, USA*

[5]*Institue of Physics of Complex Matter, École Polytechnique Fédérale de Lausanne, CH-1015 Lausanne, Switzerland*

(Received 1 September 2010; published 4 January 2011)

The transient optical conductivity of photoexcited $1T$-TaS_2 is determined over a three-order-of-magnitude frequency range. Prompt collapse and recovery of the Mott gap is observed. However, we find important differences between this transient metallic state and that seen across the thermally driven insulator-metal transition. Suppressed low-frequency conductivity, Fano phonon line shapes, and a midinfrared absorption band point to polaronic transport. This is explained by noting that the photoinduced metallic state of $1T$-TaS_2 is one in which the Mott gap is melted but the lattice retains its low-temperature symmetry, a regime only accessible by photodoping.

DOI: 10.1103/PhysRevLett.106.016401 PACS numbers: 71.45.Lr, 63.20.kd, 73.20.Mf, 78.47.jg

Low-dimensional dichalcogenides exhibit a wealth of competing phenomena, ranging from Mott and Peierls transitions [1,2] to spin and charge density waves (CDW) [3,4] and superconductivity [5]. Many such materials also display photoinduced phase transitions, wherein light pulses can create new transient states by driving ultrafast changes in the macroscopic properties [6,7].

$1T$-TaS_2 is a quasi-two-dimensional transition metal dichalcogenide in which CDW behavior coexists with strong electron-electron correlations [8–12]. At high temperatures $1T$-TaS_2 is metallic. Below 350 K, a periodic lattice distortion creates star-shaped clusters of tantalum atoms, causing the CDW to become nearly commensurate as domains of such clusters appear [5,10]. Below $T_C = 180$ K, as the CDW becomes fully commensurate with the lattice and a long-range $\sqrt{13} \times \sqrt{13}$ superlattice structure emerges [9–11], the system becomes insulating. This structural distortion reduces the bandwidth below a critical value and leads to the opening of a 100-meV correlation (Mott) gap, with electrons localized at the star centers [4,9,12]. Mott localization explains the low-temperature conductivity, which is lower than that expected from band structure [9].

The general features of the photoinduced dynamics in $1T$-TaS_2 were first revealed in all-optical studies [13–15], which highlighted important changes in the near-infrared optical properties and the excitation of coherent CDW amplitude-mode oscillations. Time-resolved photoelectron spectroscopy experiments [7] have provided a more comprehensive view of the physics, demonstrating the prompt collapse and recovery of the gap at $k = 0$ on a time scale short compared to the period of the coherent amplitude mode. This was interpreted as ultrafast melting of the Mott insulator, driven primarily by carrier temperature and only weakly influenced by the amplitude mode. Recent ultrafast electron diffraction measurements substantiate this view, showing that photodoping does not trigger complete relaxation of the structural distortion [16].

Here, we set out to probe the electrodynamics of this transient Mott-melted phase, using a combination of ultrafast optical probes that cover three decades of frequency. In this way, we access a state of the solid in which photodoping has removed the correlation gap, while the lattice symmetry, and presumably the bandwidth, of the low-temperature Mott insulator are only weakly perturbed.

In our experiments, $1T$-TaS_2 was held in its low-temperature insulating phase at 15 K and excited with 1.3 μm-wavelength pulses (950 meV) from an optical parametric amplifier. In a first set of measurements, low-energy transport was probed with time-resolved THz spectroscopy [17–19]. The time-dependent reflectivity was referenced against that of the unperturbed sample and of a gold-coated portion of the surface. This allowed for the determination of the complex optical constants for each time delay [20]. The time-dependent conductivity was extracted by considering a thin photoexcited film with an unperturbed bulk volume beneath, thereby keeping into account the mismatch in pump and probe penetration depths (45 nm and 7 μm, respectively).

Figure 1(a) shows the real part of the conductivity σ_1 obtained in the low-temperature equilibrium phase and at several pump-probe time delays for a pump intensity of 550 μJ cm^{-2}. For comparison, the pump fluence range used in earlier photoemission studies on the photoinduced phase was restricted to intensities lower than 150 μJ cm^{-2} [7]. In the conductivity data presented here, Drude-like

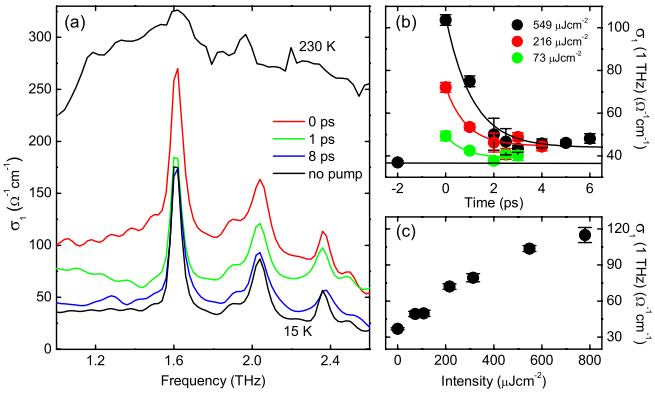

FIG. 1 (color online). (a) Real part of the conductivity σ_1 as a function of pump-probe time delay for 550 μJ cm^{-2} pump intensity. Static conductivity in the low- and high-temperature phases is shown in black for comparison (high-temperature data from [12]). (b) Transient behavior of σ_1 (1 THz) for different pump intensities (lines are guides to the eye). (c) Intensity dependence of σ_1 (1 THz) at 0 ps time delay.

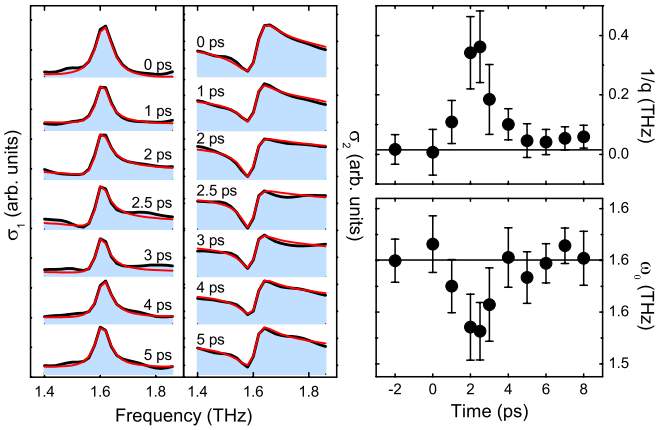

FIG. 2 (color online). Temporal evolution of the 1.6 THz mode after excitation with 550 μJ cm^{-2} pump pulse. Left-hand panels: Real and imaginary parts of the conductivity for different pump-probe delays (black lines). Gray (red) lines are fits using a Fano line shape. Right-hand panels: Time-dependent asymmetry parameter $1/q$ and renormalized mode frequency ω_0.

behavior is indicated by a flat response in σ_1. The temporal evolution of σ_1 (1 THz) is plotted in Fig. 1(b). A prompt increase is followed by exponential decay back towards equilibrium, reflecting changes in the Drude spectral weight indicative of the loss and recovery of the Mott gap [7]. However, the photoinduced change in σ_1 is significantly smaller than that observed upon heating. Furthermore, the three low-lying phonon modes observed [11,12] remain essentially unscreened and σ_1 increases continuously with excitation fluence, as shown in Fig. 1(c). All these observations are inconsistent with the larger steplike increase in σ_1 and the complete screening of the phonon modes observed at 220 K [12,21]. This indicates a transient metallic state with qualitatively different transport properties to those observed in the thermal metallic state.

Figure 2 shows the complex conductivity around the 1.6 THz phonon resonance at various time delays. We find that the Lorentzian phonon line shapes of the insulator become strongly asymmetric in the photoexcited state. The real part σ_1 exhibits a clear shift of spectral weight from the low- to the high-energy side of the mode, with a dip developing below the central frequency. The imaginary part σ_2 flattens on the high-energy side. A similar effect, though of smaller magnitude, is seen in the other two modes within our measurement bandwidth.

These asymmetries are well described by the Fano effect, a general spectroscopic feature which arises from coupling between a discrete resonance and a continuum of excitations [22]. Such coupling produces interference around the resonance, leading to a complex conductivity of the form

$$\sigma(\omega) = i\sigma_0(q - i)^2\left(i + \frac{\omega^2 - \omega_0^2}{\gamma_0\omega}\right)^{-1},$$

where ω_0 and γ_0 are the mode central frequency and linewidth, respectively, and q is the Fano asymmetry parameter ($1/q$ denotes a more asymmetric profile) [22,23]. Fano effects in phonon line shapes have been observed in other correlated electron systems both statically [23,24] and dynamically [25,26]. Their presence indicates strong electron-phonon coupling, and studying them can reveal much useful information on the interactions in correlated systems [24,27].

The gray (red) lines in Fig. 2 show a fit to the line shapes of the 1.6 THz mode as a function of pump-probe time delay. We note that the asymmetry parameter and renormalized phonon frequency, shown on the right-hand side of Fig. 2, reach their maximum alteration after around 2 ps. This is in apparent contrast with the prompt increase in low-frequency conductivity of Fig. 1. However, it is to be stressed that the temporal resolutions of the two measurements are different. The extrapolated dc conductivity is found by measurement of the broadband THz response, which can be determined on the subpicosecond time scale. On the other hand, reshaping of the phonon linewidths involves only spectral features that extend over a few hundred GHz bandwidth and, as such, cannot be detected faster than a few picoseconds.

The decay back to equilibrium of the asymmetry parameter and mode frequency exhibit the same temporal dependence as σ_1 in Fig. 1 and of the Mott gap measured in Ref. [7]. Moreover, the sign of the asymmetry shows that the phonons are interacting with a continuum centered at higher energy, likely the new states appearing as the Mott gap collapses [22,24].

At higher photon energies, photoinduced reflectance changes were measured with pulses from a second optical parametric amplifier, continuously tunable from the 100-meV Mott gap (12.4 μm wavelength) to the visible.

Figure 3 shows typical time-domain traces obtained for three different probe energies above the gap. The reflectance shows a sudden increase near zero time delay, followed by decay with superimposed 2.4-THz oscillations from the coherent CDW amplitude mode [13–15].

The magnitude of the reflectance change, the relative size of the oscillations, and their lifetime all depend on the probe photon energy, as illustrated in the inset of Fig. 3. As the probe energy is lowered towards the gap, $\Delta R/R$ increases dramatically due to the shift of spectral weight into the previously gapped region [7]. Conversely, the coherent lattice vibrations influence the optical response progressively less. This suggests that the structural distortions are only weakly connected to the low-frequency electrodynamics, further substantiating a view in which the Mott gap is melted independently from the coherent CDW distortions.

The photoinduced changes in reflectance from the THz to the visible are summarized in Fig. 4. The data were taken at 0 ps time delay, when the Mott gap has just collapsed and the reflectance changes, and hence the associated conductivity changes, are maximal. Note that while in the THz range the raw signal is small ($\ll 1\%$) due to the large difference between the pump and probe penetration depths, in the midinfrared region, where the extinction coefficients are better matched, a pronounced increase in reflectance is clearly visible already in the unprocessed data.

To extract broadband time-dependent optical conductivity in the absence of phase information at high photon energies, we applied the following procedure. First, the static broadband reflectance at 30 K was fitted by modeling the equilibrium optical conductivity with a series of Lorentzians, accounting for the phonons and electronic transition bands. Second, we analyzed the photoinduced changes in reflectivity, which could be modeled by shifts of spectral weight among the oscillators of the equilibrium fit. However, the midinfrared response required the addition of a new resonance centered at 155 meV. This feature has no analogue in any of the thermal phases. Its time dependence can be seen in the reflectance transients of Fig. 3 which give it its structure, especially the trace at 120 meV, close to the center of the absorption band. It appears promptly upon photoexcitation and has decayed after almost 1 ps, indicating a strong connection to the loss and revival of the Mott gap, which occurs on the same time scales.

The lower panel of Fig. 4 shows the broadband conductivity of the photoinduced phase at 0 ps time delay, as determined by this procedure. Three features emerge as especially meaningful: reduced low-frequency conductivity compared to the high-temperature phase, Fano line shapes for the phonons, indicative of strong electron-lattice coupling, and a transient midinfrared resonance. The nature of this midinfrared band is consistent with that of polaron bands in other strongly correlated materials [28,29], and the asymmetric reshaping in the phonon line shapes emphasizes strong coupling between electrons and the lattice coinciding with the appearance of this new feature.

From the combined observations above, then, the key conclusion of our work is that transport in the photoinduced phase is polaronic. Microscopically, charges that in

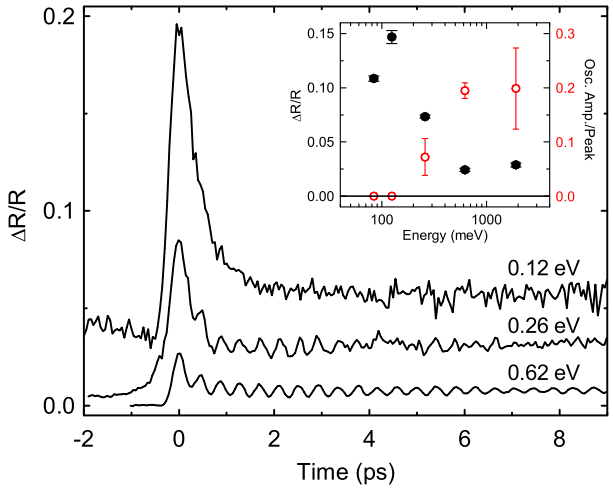

FIG. 3 (color online). Pump-probe traces for three probe photon energies. Inset: Peak reflectivity changes ($\Delta R/R$) as a function of probe photon energy (black dots, left-hand axis) and ratio of oscillation amplitude to peak $\Delta R/R$ (red circles, right-hand axis). In all cases the pump intensity was $\sim 750\ \mu\mathrm{J\,cm^{-2}}$.

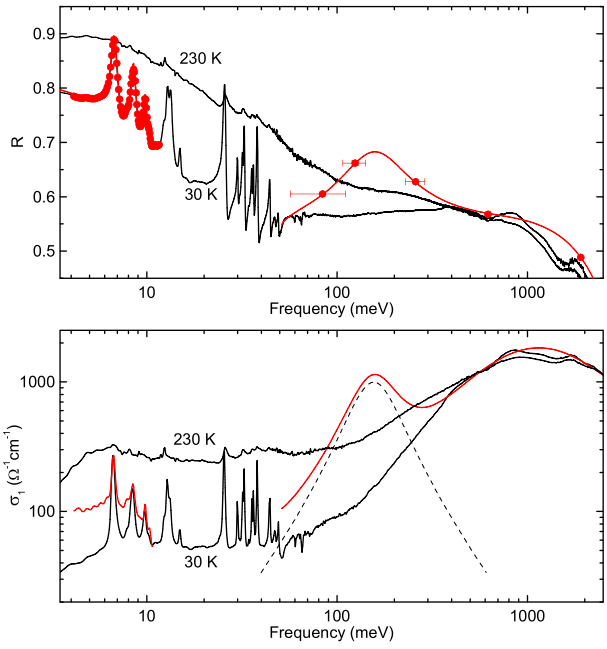

FIG. 4 (color online). Upper panel: Reflectance change immediately after photoexcitation (red dots). Gray (red) line is a fit to the data (see text). Lower panel: Calculated conductivity immediately after photoexcitation [gray (red) line]. Dashed black line is a Lorentzian representing a polaron band. In both panels, continuous black lines are the reflectance and conductivity of the thermal phases [12].

the ground state were localized by electron correlations are made mobile after photodoping, although electron-lattice coupling, which is still strong due to the presence of the CDW, imposes a dominant energy scale on their transport. These features belong to an exotic state of $1T$-TaS_2 that is only accessible with photodoping.

In summary, we have used optical spectroscopy over a broad frequency range to measure the transport properties of photoexcited $1T$-TaS_2. Our data clearly indicate the formation of a new state, with polaronic transport that descends directly from the separate influence that light has on electron correlations and on the lattice response. As such, the use of ultrabroadband time-resolved optical spectroscopy emerges as an indispensable tool to understand the role of many interacting degrees of freedom in transient states of complex matter.

*Corresponding author.
n.dean1@physics.ox.ac.uk
†Corresponding author.
andrea.cavalleri@mpsd.cfel.de

[1] P. Fazekas and E. Tosatti, Physica (Amsterdam) **99B**, 183 (1980).
[2] S. van Smaalen, Acta Crystallogr. Sect. A **61**, 51 (2004).
[3] G. Grüner, *Density Waves in Solids* (Perseus, Cambridge, MA, 1994).
[4] F. Clerc, C. Battaglia, H. Cercellier, C. Monney, H. Berger, L. Despont, M. G. Garnier, and P. Aebi, J. Phys. Condens. Matter **19**, 355002 (2007).
[5] B. Sipos, A. F. Kusmartseva, A. Akrap, H. Berger, L. Forro, and E. Tutis, Nature Mater. **7**, 960 (2008).
[6] F. Schmitt *et al.*, Science **321**, 1649 (2008).
[7] L. Perfetti, P. A. Loukakos, M. Lisowski, U. Bovensiepen, H. Berger, S. Biermann, P. S. Cornaglia, A. Georges, and M. Wolf, Phys. Rev. Lett. **97**, 067402 (2006); L. Perfetti, P. A. Loukakos, M. Lisowski, U. Bovensiepen, M. Wolf, H. Berger, S. Biermann, and A. Georges, New J. Phys. **10**, 053019 (2008).
[8] J. A. Wilson, F. J. DiSalvo, and S. Mahajan, Adv. Phys. **24**, 117 (1975).
[9] P. Fazekas and E. Tosatti, Philos. Mag. B **39**, 229 (1979).
[10] F. Clerc, C. Battaglia, M. Bovet, L. Despont, C. Monney, H. Cercellier, M. G. Garnier, P. Aebi, H. Berger, and L. Forro, Phys. Rev. B **74**, 155114 (2006).
[11] S. Uchida and S. Sugai, Physica (Amsterdam) **105B**, 393 (1981).
[12] L. V. Gasparov, K. G. Brown, A. C. Wint, D. B. Tanner, H. Berger, G. Margaritondo, R. Gaal, and L. Forro, Phys. Rev. B **66**, 094301 (2002).
[13] J. Demsar, L. Forró, H. Berger, and D. Mihailovic, Phys. Rev. B **66**, 041101 (2002).
[14] Y. Toda, K. Tateishi, and S. Tanda, Phys. Rev. B **70**, 033106 (2004).
[15] T. Onozaki, Y. Toda, S. Tanda, and R. Morita, Jpn. J. Appl. Phys. **46**, 870 (2007).
[16] M. Eichberger, H Schäfer, M. Krumova, M. Beyer, J. Demsar, H. Berger, G. Moriena, G. Sciaini, and R. J. Dwayne Miller, Nature (London) **468**, 799 (2010).
[17] M. C. Nuss, P. M. Mankiewich, M. L. O'Malley, E. H. Westerwick, and P. B. Littlewood, Phys. Rev. Lett. **66**, 3305 (1991).
[18] M. C. Beard, G. M. Turner, and C. A. Schmuttenmaer, J. Appl. Phys. **90**, 5915 (2001).
[19] E. Knoesel, M. Bonn, J. Shan, and T. F. Heinz, Phys. Rev. Lett. **86**, 340 (2001).
[20] S. Nashima, O. Morikawa, K. Takata, and M. Hangyo, Appl. Phys. Lett. **79**, 3923 (2001).
[21] A. Thompson, R. F. Gamble, and J. F. Revelli, Solid State Commun. **9**, 981 (1971).
[22] U. Fano, Phys. Rev. **124**, 1866 (1961).
[23] I. Kezsmarki, N. Hanasaki, K. Watanabe, S. Iguchi, Y. Taguchi, S. Miyasaka, and Y. Tokura, Phys. Rev. B **73**, 125122 (2006).
[24] S. Lupi, M. Capizzi, P. Calvani, B. Ruzicka, P. Maselli, P. Dore, and A. Paolone, Phys. Rev. B **57**, 1248 (1998).
[25] M. Hase, J. Demsar, and M. Kitajima, Phys. Rev. B **74**, 212301 (2006).
[26] J. D. Lee, J. Inoue, and M. Hase, Phys. Rev. Lett. **97**, 157405 (2006).
[27] A. Damascelli, K. Schulte, D. van der Marel, and A. A. Menovsky, Phys. Rev. B **55**, R4863 (1997).
[28] S. Lupi, P. Maselli, M. Capizzi, P. Calvani, P. Giura, and P. Roy, Phys. Rev. Lett. **83**, 4852 (1999).
[29] S. Ciuchi and S. Fratini, Phys. Rev. B **77**, 205127 (2008).